HHS Public Access

Author manuscript

J Am Chem Soc. Author manuscript; available in PMC 2025 February 12.

Published in final edited form as:

J Am Chem Soc. 2025 January 15; 147(2): 2148–2157. doi:10.1021/jacs.4c16271.

O_2 Activation and Enzymatic C-H Bond Activation Mediated by a Dimanganese Cofactor

Chang Liu[a], **Guodong Rao**[b], **Jessica Nguyen**[a], **R. David Britt**[b], **Jonathan Rittle**[a,*]

[a]Department of Chemistry, University of California, Berkeley, Berkeley, California 94720, United States

[b]Department of Chemistry, University of California, Davis, Davis, California 95616, United States

Abstract

Dioxygen (O_2) is a potent oxidant used by aerobic organisms for energy transduction and critical biosynthetic processes. Numerous metalloenzymes harness O_2 to mediate C-H bond hydroxylation reactions, but most commonly feature iron or copper ions in their active site cofactors. In contrast, many manganese-activated enzymes – such as glutamine synthetase and isocitrate lyase – perform redox neutral chemical transformations and very few are known to activate O_2 or C-H bonds. Here we report that the dimanganese-metalated form of the cambialistic monooxygenase SfbO (Mn_2-SfbO) can efficiently mediate enzymatic C-H bond hydroxylation. The activity of the dimanganese form of SfbO towards substrate hydroxylation is comparable that of its heterobimetallic Mn/Fe form but exhibits distinct kinetic profiles. Kinetic, spectroscopic and structural studies invoke a mixed-valent dimanganese cofactor ($Mn^{II}Mn^{III}$) in O_2 activation and evidence a stoichiometric role for superoxide in maturing an O_2-inert Mn^{II}_2 cofactor. Computational studies support a hypothesis wherein superoxide addition to the Mn^{II}_2 cofactor installs a critical bridging hydroxide ligand that stabilizes higher-valent manganese oxidation states. These findings establish the viability of proteinaceous dimanganese cofactors in mediating complex, multistep redox transformations.

Graphical Abstract

*Corresponding Author rittle@berkeley.edu.

Author Contributions

The manuscript was written through contributions of all authors. All authors have given approval to the final version of the manuscript.

Supporting Information. Experimental and computational procedures, analytical data, X-ray diffraction data, DFT coordinates. This material is available free of charge via the Internet at http://pubs.acs.org.

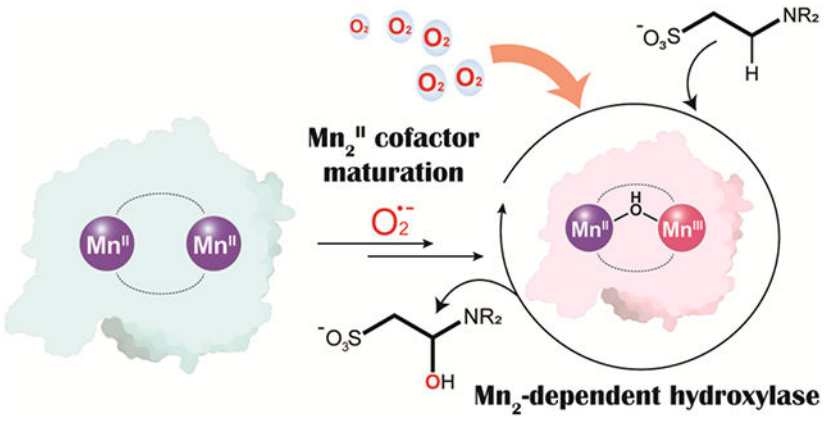

INTRODUCTION

Enzymatic C-H bond activation is essential for many biological processes, including nutrient acquisition, cellular signaling, natural product biosynthesis and xenobiotic metabolism.[1-5] Only a handful of cofactors are known to mediate these processes owing to complex catalytic cycles that often involve multiple electron- and group transfer steps. Diiron and dicopper clusters, present in many well-studied hydroxylases, possess the electronic and geometric flexibility required to satisfy these tall mechanistic demands.[6-8] In contrast, dimanganese clusters are not known to mediate catalytic C-H bond activation processes in biological systems, a likely consequence of the pronounced kinetic and thermodynamic stability of the bioavailable manganese(II) ion. In very few cases, Mn cofactors are known to mediate O_2- and/or C-H bond activation but include those cofactors in certain catechol-cleaving dioxygenases and manganese lipoxygenase.[9-15] In the rare cases where catalytic or stoichiometric C-H bond activation and/or O_2 activation processes are mediated directly by a manganese-containing cofactor, a second redox-active element is often present, such as the manganese-iron active sites found in class Ic ribonucleotide reductase β-subunits (RNR-β Ic), R2lox, and the 2-amino-isobutyric acid hydroxylase AibH1H2.[16-18]

In two established enzymatic systems where dimanganese cofactors mediate redox processes, they act on, or must be matured by reactive oxygen species (ROS) in dimanganese catalase and the class Ib/Id ribonucleotide reductase β-subunits (RNR-β Ib/Id), respectively.[19-21] In manganese catalase, a dimanganese(II) (Mn_2^{II}) cofactor reduces one equivalent of hydrogen peroxide to form a Mn_2^{III} cofactor, that subsequently oxidizes another H_2O_2 molecule (Figure 1A) to return the cofactor to its Mn_2^{II} oxidation state. In RNR-β Ib and Id, a Mn_2^{II} cofactor reacts with superoxide to form a $Mn^{III}Mn^{IV}$ cofactor, which either oxidizes a proximal tyrosine (RNR-β Ib) or directly (RNR-β Id) mediates hole transfer to the RNR α-subunit (Figure 1B).[22] In neither case is a dioxygen activation event implicated in the consensus enzymatic- or cofactor activation mechanisms. Similarly, very few synthetic non-porphyrinoid Mn complexes are known to react with O.[23,24] Yet, numerous Mn-based catalysts serve in alkane and alkene oxidations in the presence of peroxides or peracids,[25,26] and certain oxidized Mn_2 complexes stoichiometrically activate C-H bonds.[27] Given these collective observations, one might conclude that biological Mn_2

cofactors are generally inert to O_2 but, upon suitable activation, can mediate challenging oxidation reactions.

Recently, we demonstrated the sulfonate β-monooxygenase (SfbO) from *Litorolinea aerophila* (Uniprot ID:A0A540VG95) is a cambialistic monooxygenase that performs catalytic C-H bond hydroxylation reactions with either a Mn/Fe or Fe_2 cofactor, but is most active with the former cofactor.[28] While the native substrate of SfbO remains unknown, this enzyme was previously reported to convert the 2-aminoethylsulfonate functional group of piperazine-*N,N'*-bis(2-ethanesulfonic acid) (PIPES) to sulfoacetaldehyde (SA) (Figure 2).[28] We proposed that this reaction proceeded via C-H bond hydroxylation by the dimetal cofactor of SfbO to furnish an unstable hemiaminal that spontaneously hydrolyses to generate SA. The unusual preference for a Mn/Fe cofactor is comparable to another amidohy-drolase-related dinuclear oxygenase (ARO), AibH1H2, which requires a Mn/Fe cofactor for 2-aminoisobutyric acid hydroxylation.[18] While very few ARO's have been experimentally scrutinized, these representative enzymes suggest that the underlying protein structure present within this enzyme family engenders Mn-containing cofactors with unique biological activity. Curiously, some SfbO reaction assays performed in the absence of iron exhibited appreciable catalytic activity suggesting that Mn_2-metallated forms of SfbO might prove comparably reactive. Herein, we report biochemical, structural, and spectroscopic studies on Mn_2-metallated SfbO that support monooxygenase activity by a Mn_2 cofactor embedded within a natural enzyme. We demonstrate that the $Mn^{II}Mn^{III}$ redox state of the cofactor – and not the Mn_2^{II} state – is competent for rapid dioxygen activation (Figure 1C).

RESULTS AND DISCUSSION

Establishment of Monooxygenase Activity by Mn_2-SfbO

We first sought to establish the reactivity of SfbO in the presence of variable amounts of Mn^{II} and Fe^{II} to quantify the impact of the available metal ions on the enzymatic activity. To generate all of the possible $Mn_xFe(2-x)$-metalated forms of SfbO *in situ*, *apo*-SfbO[28] was either (a) combined directly with a solution containing a premixed ratio of Mn^{II} and Fe^{II}, (b) metalated via sequential addition of solutions containing Mn^{II} and then Fe^{II} or (c) via sequential addition of solutions containing Fe^{II} and then Mn^{II} under anaerobic conditions at a total of 2 metal equivalents per SfbO monomer. These solutions were then combined with aerobic assay solutions containing PIPES and sodium ascorbate and allowed to incubate for 3 hours. The resultant metal-dependent-enzymatic activity profiles (Figure 3A-C) illustrated that maximal SA production was highly dependent on the manner of metal ion exposure.

Comparable studies performed on RNR and R2LOX highlight that the metal binding dynamics of enzymes containing $Fe_xMn_{(2-x)}$ cofactors (x = 0-2) is often highly dependent on the metalation protocol.[16,17,29] Similar experiments performed on proteins that require a Mn/Fe cofactor, such as *C. trachomatis* RNR-β Ic, returned metal:activity trends loosely comparable to the data shown in Fig 3A and Fig 3B, but not Fig 3C. Unlike SfbO, *C. trachomatis* RNR-β Ic is not reported to be cambialistic and was found to display marginal catalytic activity in the presence of homobimetallic cofactors.[16] The complexity observed for metal-dependent SA production by SfbO (Fig 3) partially stems from its highly asymmetric active site (Fig 2): Site 1 is expected to bind metals more tightly than Site 2

owing to its greater number of available protein-derived ligands. We hypothesize that the order of metal addition will therefore strongly influence the metal content of these sites and that the first metal added to *apo*-SfbO will preferentially occupy Site 1. *Importantly, regardless of the divergent metal-dependent SA production at intermediate ratios of Fe:Mn, the SA generation in assays devoid of available Fe ions were found to be nonzero*. In fact, SA production by SfbO in the presence of 2 equiv Mn^{II} was always found to be greater than in the presence of 2 equiv Fe^{II}. This suggests that a Mn_2-metalated form of SfbO may be competent for this enzymatic reaction (Figure 2).

Biological Mn_2 cofactors are not known to mediate the activation of O_2 or C-H bonds, yet both of these processes are implied by the *in-situ* activity of SfbO. Since the Mn_2 cofactors present in RNR-β Ib/Id and Mn-catalase are known to react with superoxide and hydrogen peroxide (Figure 1), respectively, we assessed the potential involvement of these ROS in the SfbO-mediated enzymatic reaction. *Apo* SfbO was combined with two equivalents of Mn^{II} and subjected to standard assay conditions in the presence or absence of catalase and/or superoxide dismutase (SOD). The resultant data (Figure 3D) indicated that maximal SA production was observed in the presence of both catalase and SOD, indicating that neither hydrogen peroxide nor superoxide represented the sacrificial oxidant in these mixtures (*vide infra*). Negligible SA was produced when SfbO was removed from these assays (Figure S1). This control experiment indicates that unbound Mn^{II}, catalase and/or SOD are not responsible for the measured SA production. Thus, the available data suggested that the presence of SOD and catalase enhanced the catalytic competence of Mn_2-SfbO and we speculate that prolonged exposure to ROS may damage either the embedded Mn_2 cofactor or the surrounding protein structure under these assay conditions. The protective effects of catalase and SOD were evaluated by monitoring time-dependent SA production. The presence of catalase appreciably extended the catalytic performance of Mn_2-SfbO (Figure S1). The addition of 1 mM H_2O_2 to assay mixtures was also found to abolish the SA production and supports our hypothesis that H_2O_2 serves to deactivate SfbO. Since assays performed under anaerobic conditions generated negligible quantities of SA (Figure 3D), the available data supports the notion that Mn_2-SfbO functions as an O_2-dependent enzyme.

Since iron contamination could be non-negligible in biochemical reagents and plasticware, it is difficult to rigorously exclude this metal ion from any routine biochemical assay. Indeed, early studies on the N-oxygenase AurF advocated for a dimanganese active site,[30] but were later debunked after rigorous metalation studies.[31] Hence, we considered the possibility that the apparent activity of Mn_2-SfbO stemmed from the generation of sufficient Mn/Fe-metalated SfbO to obscure the catalytic results. However, evidence against this proposal was gleaned from an analysis of the apparent kinetic isotope effect (KIE) observed for C-H bond cleavage of the PIPES substrate by SfbO. Assays performed with Mn/Fe-SfbO and d_{18}-PIPES confirmed that a C-H/D bond cleavage step contributes to k_{cat}, as >10 fold less product was generated as compared to otherwise identical assays that employed unlabeled PIPES as a substrate.[28] Since the K_M parameters for Mn/Fe-SfbO and Mn_2-SfbO with unlabeled PIPES are similar and rather large (> 50 mM) (Figure 3E), simple competition assays performed in the presence of equimolar amounts of PIPES and d_{18}-PIPES should allow for the apparent KIE determination of C-H/D bond cleavage at $[PIPES]_{total}$ = 300 mM.[32] Productive enzymatic activity directed at PIPES or d_{18}-PIPES is

expected to furnish d_0-SA or d_1-SA, respectively, as the dominant product isotopologues and these products are readily quantified by LC-MS analysis of derivatized assay mixtures (Figure 3F and Figure S2). Identical competition assays performed with Mn_2- or Mn/Fe-SfbO generated different relative amounts of these SA isotopologues (functionalized with 2,4-dinitrophenylhydrazine, DNPH) which reflect apparent KIEs of 7.4 ±0.5 and 10.0 ± 0.3, respectively. The significant difference ($p = 0.0015$) in these values requires the presence of mechanistically-distinct C-H/D cleaving intermediates in Mn_2- and Mn/Fe-SfbO preparations.[33] These results, therefore, diminish the possibility that contaminating Mn-Fe cofactors substantially contribute to the enzymatic activity of Mn_2-SfbO preparations, and indicate that the Mn_2 cofactor in SfbO is capable of mediating catalytic C-H bond cleavage processes.

Mechanistic Studies of the Dimanganese Cofactor in SfbO.

X-band Electron Paramagnetic Resonance (EPR) spectra of *apo* SfbO metalated with two equivalents of Mn^{II} under anaerobic conditions revealed signals originating from three distinct paramagnetic species (Figure 4A, top). Sharp features near g~2 were readily assigned to $Mn(OH_2)_6^{2+}$,[17] and a multiline signal at g~4 is consistent with a mononuclear Mn^{II} ion in a low-symmetry coordination environment.[9,10,34] We tentatively assign this latter species to singly-metalated Mn-SfbO. Broad features (denoted with asterisks) that span a range of magnetic fields from 200 to 440 mT are comparable to spectra reported for the Mn_2^{II}-form of bacteriophage λ phosphatase and synthetic model systems.[35,36] These signals can be ascribed to excited state transitions of weakly-antiferromagnetically coupled Mn_2 clusters and often lack observable ^{55}Mn hyperfine coupling in X-band spectra. These features were negligible when apo-SfbO was reconstituted with 1 equivalent of Mn^{II} anaerobically, and the multiline g~4 signal intensity was enhanced (Figure S4). The addition of a second equivalent of Mn^{II} to these samples diminished the g~4 signal and generated the broad Mn_2^{II} features (Figure S4). In all of these spectra, the presence of unbound $Mn(OH_2)_6^{2+}$ reflects thermodynamic and kinetic lability of the Mn^{II} ions with SfbO. Representative Mn^{II} dissociation constants (K_D) for proteins containing similar coordination environments to that of the SfbO active site are typically in the 1-30 μM range[37] and since these EPR samples contained ~200 μM SfbO, the observation of signals ascribed to $Mn(OH_2)_6^{2+}$ is expected and frequently observed in studies of other Mn^{II}-binding proteins (reference 35 provides a particularly illustrative example).

Overnight exposure of the sample to air resulted in subtle spectral changes with slightly decreased intensity of the broad features (Figure 4A, middle). Interestingly, when comparably generated samples were exposed to sodium ascorbate and PIPES substrate under air to emulate catalytic assay conditions, a new multiline signal was observed underneath the persistent $Mn(OH_2)_6^{2+}$ features (Figure S5A) but exhibited wider spectral breadth and complexity. The signal intensity associated with this new species was enhanced when air-oxidized Mn_2-SfbO preparations (exposed to air for ~3 days) were rendered anaerobic and subsequently exposed to 5 mM sodium ascorbate (Figure S5B) or 20 mM sodium dithionite (DT) (Figure 4A, bottom), suggesting that this species was generated via the reduction of an *in situ*-generated, EPR silent species such as an antiferromagnetically coupled Mn_2^{III} or Mn_2^{IV} cofactor.

Further analysis of the DT-reduced species by pulsed Q-band EPR enabled the resolution of hyperfine coupling to two I = 5/2 ^{55}Mn nuclei (Figure 4B). Simulation of this signal revealed an axial **g** tensor (2.03, 1.98, 1.98) and two ^{55}Mn hyperfine coupling tensors $\mathbf{A_{Mn1}}$ [(265, 252, 250) MHz] and $\mathbf{A_{Mn2}}$ [(135, 126, 126) MHz], which collectively support the presence of either an antiferromagnetically coupled $Mn^{II}Mn^{III}$ or $Mn^{III}Mn^{IV}$ cofactor. Previously reported EPR spectra for other mixed-valent Mn_2 cofactors and complexes are sufficiently variable to preclude unambiguous oxidation state assignment solely based on hyperfine parameters.[20,21,38-40] However, since this species was only found to accumulate upon treatment with a chemical reductant, we favor a $Mn^{II}Mn^{III}$ formulation. Curiously, the EPR features arising from this mixed-valent species proved stable at room temperature for 72 hours in the presence of 20 mM sodium dithionite (Figure S5C), suggesting that further reduction to a Mn_2^{II} state is kinetically inhibited and is suggestive of key structural differences between these redox forms (*vide infra*).

These observations raise an important question: *how* is the Mn_2^{II} cofactor of SfbO matured into the catalytically competent redox forms involved in enzymatic catalysis? In RNR-β Ib and Id the critical $Mn^{III}Mn^{IV}$ intermediate is not generated from O_2 directly, but instead via stoichiometric superoxide activation at a Mn_2^{II} precursor.[20-22] Accordingly, we speculated that one or more ROS may be necessary to prime the Mn_2^{II} SfbO for subsequent O_2-dependent catalytic turnovers. Exposure of Mn_2^{n}-SfbO to H_2O_2 does not detectably perturb the UV/visible absorption features of Mn_2^{II}-SfbO (Figure S7B) and no detectable SA is generated upon exposure of Mn_2^{II}-SfbO to H_2O_2 (Figure S1), ruling out this ROS in cofactor maturation.

Kinetic evidence supporting a role for superoxide in cofactor maturation includes a pronounced impact of SOD on the initial rate of SA production by SfbO (Figure 5). When enzymatic assays of *apo* SfbO reconstituted with 2 equivalents of Mn^{II} were performed in the presence of PIPES and catalase (to remove adventitiously-generated H_2O_2), the formation rate of the SA product was linear over the first 20 minutes of the assay. In contrast, assays solutions that additionally contained SOD (to remove adventitiously-generated O_2^-) generated much less SA during the first 5 minutes of the assay conditions. The addition of increasing amounts of SOD to the assay mixtures (up to 1 mg/mL) was found to reduce SA production in assays quenched after 8 minutes by ~60% (Figure S8). In contrast, varying the catalase concentration (Figure S9) had no significant impact on the SA production within an 8-minute assay. Following this induction period, however, the SA formation rate was indistinguishable from assays performed in the absence of SOD. These data suggest that superoxide was transiently accumulated under these assay conditions and may be necessary for Mn_2-SfbO to gain catalytic competence.

Superoxide is known to be continuously generated in aerobic aqueous solutions of tertiary amines (e.g., HEPES).[41,42] The ascorbate employed in the reaction assays is also known to furnish superoxide in the presence of oxygen.[43,44] Collectively, we propose that these two established chemical reactions accumulate sufficient superoxide to mature the dimanganese cofactor of Mn^{II}-SfbO upon initiation of the assay (<5 min, Figure 5). We note that the time scale of these initial rate studies represents only a small fraction of the typical assay time (180 minutes). We speculate that the moderate protective effects of SOD on the SfbO

catalysis measured at this latter time point (Figure 3D) originate from the mitigation of another, presently unknown detrimental reaction of superoxide with Mn_2-SfbO.

Probing the direct reaction of Mn_2^{II}-metalated SfbO with superoxide is challenged by the millisecond half-life of this ROS in aqueous solution.[45] Thus, we investigated photoredox-mediated means of *in situ* superoxide generation. Superoxide is reliably generated with ruthenium(II)-tris-bipyridine ($Ru(bpy)_3^{2+}$) upon reductive quenching of photoexcited $Ru(bpy)_3^{2+}$ with tri-alkylamines in the presence of O_2.[46] We monitored the UV/visible absorption spectra of solutions containing 430 μM Mn_2^{II}-SfbO, 5 mM iPr_2NEt, 5 μM $Ru(bpy)_3^{2+}$ (Figure 6A) during the course of LED lamp illumination aerobically at ambient temperature. New visible absorption features extending from 300 to 600 nm were evident following 120 minutes of illumination and may be ascribed to charge transfer bands stemming from an oxidized Mn_2 cofactor. These features are comparable to those of the Mn_2^{III} forms of class Ib RNR and dimanganese catalase[20,47]. In contrast, minimal spectral changes were observed when these experiments were repeated in the presence of SOD (Figure 6B). When similarly prepared solutions were analyzed by X-band EPR spectroscopy, the broad features ascribed to the Mn_2^{II} cofactor were diminished in a light-dependent fashion (Figure 6C). Importantly, Mn_2-SfbO samples subjected to this photoredox protocol retain 80% activity for SA production as compared to standard enzyme assays (Figure S10), indicating that this process does not deactivate the enzyme. The $Mn^{II}Mn^{III}$ form of Mn_2-SfbO samples subjected to this photoredox protocol exhibit identical spectra those obtained from air-oxidized samples (Figure S11).

Notably, no additional EPR signals were generated under these conditions, consistent with the net oxidation of Mn_2^{II}-SfbO by superoxide by two electrons to furnish Mn_2^{III}-SfbO. While further investigation will be required to understand this unbalanced chemical reaction, these data support the plausibility of superoxide-mediated cofactor maturation in SfbO. We speculate that Mn_2^{II}-SfbO can efficiently scavenge free superoxide owing to the solvent-accessible nature of the active site (PDB: 9BU9). This is in stark contrast to the buried active site in RNR-β Ib which requires a dedicated flavodoxin to specifically deliver superoxide for cofactor activation.[22] A similar trend was also observed in RNR-β Id that utilizes free superoxide for cofactor activation.[21]

Further UV/visible investigations (Figure 7) reveal unexpected reactivity profiles of the various cofactor redox states. The UV-visible features of Mn_2^{III}-SfbO were diminished upon anaerobic titration with a total of 0.4 equivalents of DT (0.8 electrons/SfbO) (Figure 7A) consistent with formation of the EPR-active $Mn^{II}Mn^{III}$ redox form. This electron inventory and weak absorbance of the product best supports a $Mn^{II}Mn^{III}$ redox state rather than $Mn^{III}Mn^{IV}$, since the latter species is expected to display strong absorption features near 400 nm ($\varepsilon \sim 3\ mM^{-1}\ cm^{-1}$).[21] Similar to that found via EPR analyses, prolonged DT exposure does not detectably affect these UV/visible features. However, exposure of these $Mn^{II}Mn^{III}$-SfbO preparations to air regenerated the Mn_2^{III} absorption features within minutes, coupled with disappearance of the $Mn^{II}Mn^{III}$ EPR signal, suggestive of dioxygen activation by this redox form (Figure 7B, Figure S5D). As previously reported,[28] the UV/visible spectrum of anaerobically prepared Mn_2^{II}-SfbO is essentially featureless at wavelengths >300 nm. No obvious spectral change was observed following ~1 hour of air exposure (Figure

7C), in stark contrast to the relatively rapid O_2 reactivity of $Mn^{II}Mn^{III}$-SfbO preparations. Collectively, these results suggest that the $Mn^{II}Mn^{III}$ redox state is kinetically competent for catalytic O_2 activation by Mn_2-SfbO, and the inert nature of the Mn_2^{II} form excludes its participation as a catalytically-viable intermediate.

Structural Characterization of the Mn_2^{II} and $Mn^{II}Mn^{III}$ Co-factors.

There are only a handful of dinuclear metalloproteins known to stabilize Mn ions in oxidations states >2, and include the class 1 RNR's, R2lox, manganese catalase, and AibH2. All of these active sites, like that in SfbO (Figure 2) share a combination of histidine, glutamate and aspartate-derived ligands, yet exhibit distinct enzymatic chemistry.[16-21] Since the available spectroscopic data suggested that the one-electron interconversion of Mn_2^{II}, and $Mn^{II}Mn^{III}$ forms of SfbO was unusually sluggish, we examined their structural differences with X-ray crystallography coupled with computational investigations. Single crystals of SfbO enriched in these cofactor redox forms diffracted to <1.4 Å resolution allowing for insightful structural comparisons. We note, however, that the occupancy of some Mn and aquo atoms are partial (50-80%) owing to the expected micromolar dissociation constants for Mn^{II} and this might distort bond metrics and merit computational validation (vide infra). Globally, both structures (PDB: 9BU9 and 9BUA) exhibited a high degree of structural similarity (RMSD: 0.22 Å, over all non-solvent atoms) but the active site dimanganese cofactors (Figure S12) exhibited salient differences (Table S3). Three aquo ligands (with undetermined protonation states, investigated computationally below) were observed in the $Mn^{II}Mn^{III}$ form (Figure 8A), including one well-resolved bridging ligand. In contrast, no bridging aquo ligand is apparent in the $2F_O$-F_C map of Mn_2^{II} form (Figure 8B) and attempts to model such a ligand resulted in the appearance of appreciable negative density in the resultant F_O-F_C maps (Figure S13). Thus, each Mn ion in the Mn_2^{II} form is 5-coordinate with coordination geometries best characterized as distorted (τ_5 = 0.47) and idealized (τ_5 = 0.01) square pyramidal for the Site 1 and Site 2 Mn ions, respectively. Since the Mn ions in the $Mn^{II}Mn^{III}$ redox form exhibited 6-coordinate pseudo-octahedral geometries, formal one-electron oxidation of the Mn_2^{II} cofactor requires concomitant installation of the bridging aquo ligand. We speculate that these structural differences may explain the kinetic stability of the $Mn^{II}Mn^{III}$ redox form to excess DT and that the superoxide maturation process may critically serve to install the bridging aquo ligand.

Insight into the protonation states of the aquo ligands in the $Mn^{II}Mn^{III}$ redox form was gleaned from gas-phase Density Functional Theory (DFT) computations on truncated active site models (Figure 9A, Supporting Information). Optimized gas-phase geometries of the dimanganese cofactor were obtained considering a combination of bridging O^{2-}- or OH^- ligands and either a terminal H_2O or OH^- ligand positioned adjacent to ^{342}D (truncated schematics of these models are depicted in Figure 9B). The resultant Broken Symmetry wavefunctions consistently localized the d^4 Mn^{III} ion to Site 2 as evidenced by a Jahn-Teller axial compression of two aquo ligands in all models. The computational model harboring a bridging O^{2-} ligand exhibited notable discrepancies with the experimental bond metrics, including overly short Mn···Mn and Mn-(μ-O) distances. In contrast, the corresponding metrics for models containing bridging OH^- ligands were in good agreement with the

experimental data. For comparison, manganese catalase crystallized in its Mn_2^{III} states is known to contain one bridging O^{2-} ligand and exhibits a far shorter Mn···Mn distances of 3.0-3.2 Å.[48] Thus, the long intermetallic distance observed in $Mn^{II}Mn^{III}$-SfbO reflects the absence of a bridging oxo ligand.

Experimentally, the Site 2 aquo ligand positioned *trans* to the bridging hydroxide ligand was found to engage in a strong hydrogen bonding interaction with the carboxylate of ^{342}D and exhibited a much shorter Mn-O distance than the *cis* terminal aquo ligand (Figure 9B). We thus considered the possibility of a terminal OH^- ligand at the former position. The corresponding metrics for optimized models that contained either a terminal aquo or a hydroxide ligand were consistent with the experimental bond distances within one standard deviation. Owing to this ambiguity and the partial occupancies of the Mn ions (50-80%) in the crystal structure, we are hesitant to assign the protonation state of this terminal aquo ligand. Collectively, these structural investigations highlight the subtle importance of a bridging hydroxide ligand in stabilizing partially-oxidized dimanganese cofactors, and mediating redox chemistry necessary for O_2 activation.

While a detailed mechanism for C-H bond hydroxylation by Mn_2-SfbO remains unknown, we speculate that O_2 binding to $Mn^{II}Mn^{III}$-SfbO would likely furnish a dimanganese(III)-superoxide intermediate (or a redox isomer) that might be directly competent for C-H bond activation. Such a scenario is related to the mixed-valent $Fe^{II}Fe^{III}$ cofactors of PhnZ, MIOX and MbnBC that, upon O_2 coordination, utilize diiron(III)-superoxo intermediates to abstract the C-H bonds of their respective substrates.[49-52] Subsequent steps of the SfbO mechanism are complicated by the possible involvement of ensuing higher-valent intermediates and the apparent requirement of additional electron equivalents to convert PIPES to SA. The combination of freshly-prepared $Mn^{II}Mn^{III}$-SfbO with an aerobic assay mixture lacking ascorbate furnished negligible SA (Figure S14). Mn_2^{III}-SfbO was similarly found to be incompetent for stoichiometric SA generation (Figure S14) and these experiments collectively suggest that Mn_2-SfbO requires an additional electron to complete its catalytic cycle. Without knowledge of the timing of this reduction process, however, we hesitate to further speculate on the mechanism of SA formation by Mn_2-SfbO.

CONCLUSIONS

The available catalytic and spectroscopic data collected on Mn_2-SfbO implicate a dimanganese cofactor that can perform O_2 activation, stoichiometric chemical reduction and C-H bond activation processes. These individual catalytic steps have rarely been observed at synthetic Mn_2 clusters, and are jointly unprecedented within natural Mn_2-dependent enzymes. Our studies here highlight an unusual role of superoxide in maturing a Mn_2^{II} cluster to one that is redox-active and upon reduction to a $Mn^{II}Mn^{III}$ state can subsequently activate O_2 in situ. While this superoxide maturation process draws clear parallels to those cofactors in RNR-β Ib/Id, it is noteworthy that Mn ions are more commonly associated with superoxide dismutation in, e.g., Mn-SOD[53] and phosphate-ligated Mn ions.[54] Hence, the contrasting ability of Mn_2-SfbO to assimilate this ROS may stem from unique structural and sequence features present within this unusual family of ARO enzymes that serve to endow manganese ions with atypical chemical reactivity.

Since, in general, the weak-field and poorly electron-donating nature of proteinaceous amino acid residues rarely permit the stabilization of Mn ion oxidation states greater than II, these same features must simultaneously serve to harness higher-valent forms of Mn that engage in the observed hydroxylation reactions. Nonetheless, our structural investigation reveal that the metal coordinating ligands observed in SfbO are not, by any means, extraordinary. The collection of imidazole, carboxylate, aquo and hydroxide ions that ligate this cofactor are commonplace in many dinuclear enzymes. This observation may suggest that other Mn_2-dependent redox enzymes – potentially from very different protein families – may be hiding in plain sight and only require some form of (electro)chemical maturation to unleash their reactivity.

Supplementary Material

Refer to Web version on PubMed Central for supplementary material.

ACKNOWLEDGMENT

We thank Nicholas Hadler and the Hartwig lab for assistance with the LCMS analyses. This work was primarily funded by the College of Chemistry at UC Berkeley (J.R., C.L., J.N.), and National Institutes of Health grants R35GM126961 (G.R., R.D.B.) and R01GM153888 (C.L., J.N., J.R.). Parts of this research were carried out at the Stanford Synchrotron Radiation Lightsource (supported by the DOE, Office of Basic Energy Sciences contract DE-AC02-76SF00515 and NIH P30-GM133894) and the Advanced Light Source (supported by the DOE, Office of Basic Energy Sciences contract DE-AC02-05CH11231 and NIH P30-GM124169-01).

REFERENCES

(1). Beeson WT; Vu VV; Span EA; Phillips CM; Marletta MA Cellulose Degradation by Polysaccharide Monooxygenases. Annu. Rev. Biochem 2015, 84 (1), 923–946. 10.1146/annurev-biochem-060614-034439. [PubMed: 25784051]

(2). Cytochrome P450; Ortiz de Montellano PR, Ed.; Springer US: Boston, MA, 2005. 10.1007/b139087.

(3). Rajakovich LJ; Zhang B; McBride MJ; Boal AK; Krebs C; Martin Bollinger J. 5.10 - Emerging Structural and Functional Diversity in Proteins With Dioxygen-Reactive Dinuclear Transition Metal Cofactors. In Comprehensive Natural Products III; Liu H-W (Ben), Begley TP, Eds.; Elsevier: Oxford, 2020; pp 215–250. https://doi.org/10.1016/B978-0-12-409547-2.14864-4.

(4). Schofield CJ; Ratcliffe PJ Oxygen Sensing by HIF Hydroxylases. Nat. Rev. Mol. Cell Biol 2004, 5 (5), 343–354. 10.1038/nrm1366. [PubMed: 15122348]

(5). Eichhorn E; van der Ploeg JR; Kertesz MA; Leisinger T. Characterization of α-Ketoglutarate-Dependent Taurine Dioxygenase from Escherichia Coli *. J. Biol. Chem 1997, 272 (37), 23031–23036. https://doi.org/10.1074/jbc.272.37.23031. [PubMed: 9287300]

(6). Merkx M; Kopp DA; Sazinsky MH; Blazyk JL; Müller J; Lippard SJ Dioxygen Activation and Methane Hydroxylation by Soluble Methane Monooxygenase: A Tale of Two Irons and Three Proteins. Angew. Chemie Int. Ed 2001, 40 (15), 2782–2807. 10.1002/1521-3773(20010803)40:15<2782::AID-ANIE2782>3.0.CO;2-P.

(7). Ng TL; Rohac R; Mitchell AJ; Boal AK; Balskus EP An N-Nitrosating Metalloenzyme Constructs the Pharmacophore of Streptozotocin. Nature 2019, 566 (7742), 94–99. 10.1038/s41586-019-0894-z. [PubMed: 30728519]

(8). Fujieda N; Umakoshi K; Ochi Y; Nishikawa Y; Yanagisawa S; Kubo M; Kurisu G; Itoh S. Copper–Oxygen Dynamics in the Tyrosinase Mechanism. Angew. Chemie Int. Ed 2020, 59 (32), 13385–13390. 10.1002/anie.202004733.

(9). Whiting AK; Boldt YR; Hendrich MP; Wackett LP; Que L. Manganese(II)-Dependent Extradiol-Cleaving Catechol Dioxygenase from Arthrobacter Globiformis CM-2. Biochemistry 1996, 35 (1), 160–170. 10.1021/bi951979h. [PubMed: 8555170]

(10). Emerson JP; Kovaleva EG; Farquhar ER; Lipscomb JD; Que L. Swapping Metals in Fe- and Mn-Dependent Dioxygenases: Evidence for Oxygen Activation without a Change in Metal Redox State. Proc. Natl. Acad. Sci 2008, 105 (21), 7347–7352. 10.1073/pnas.0711179105. [PubMed: 18492808]

(11). Que L; Widom J; Crawford RL 3,4-Dihydroxyphenylacetate 2,3-Dioxygenase. A Manganese(II) Dioxygenase from Bacillus Brevis. J. Biol. Chem 1981, 256 (21), 10941–10944. 10.1016/S0021-9258(19)68536-4. [PubMed: 6270137]

(12). Su C; Oliw EH Manganese Lipoxygenase. J. Biol. Chem 1998, 275 (21), 13072–13079. 10.1074/jbc.273.21.13072.

(13). Heshof R; Jylhä S; Haarmann T; Jørgensen ALW; Dalsgaard TK; de Graaff LH A Novel Class of Fungal Lipoxygenases. Appl. Microbiol. Biotechnol 2014, 98 (3), 1261–1270. 10.1007/s00253-013-5392-x. [PubMed: 24276623]

(14). Sharma A; Whittington C; Jabed M; Hill SG; Kostenko A; Yu T; Li P; Doan PE; Hoffman BM; Offenbacher AR 13 C Electron Nuclear Double Resonance Spectroscopy-Guided Molecular Dynamics Computations Reveal the Structure of the Enzyme–Substrate Complex of an Active, N -Linked Glycosylated Lipoxygenase. Biochemistry 2023, 62 (10), 1531–1543. 10.1021/acs.biochem.3c00119. [PubMed: 37115010]

(15). Whittington C; Sharma A; Hill SG; Iavarone AT; Hoffman BM; Offenbacher AR Impact of N -Glycosylation on Protein Structure and Dynamics Linked to Enzymatic C–H Activation in the M. Oryzae Lipoxygenase. Biochemistry 2024, 63 (10), 1335–1346. 10.1021/acs.biochem.4c00109. [PubMed: 38690768]

(16). Jiang W; Yun D; Saleh L; Barr EW; Xing G; Hoffart LM; Maslak M-A; Krebs C; Bollinger JM A Manganese(IV)/Iron(III) Cofactor in Chlamydia Trachomatis Ribonucleotide Reductase. Science (80-.). 2007, 316 (5828), 1188–1191. 10.1126/science.1141179.

(17). Griese JJ; Roos K; Cox N; Shafaat HS; Branca RMM; Lehtiö J; Gräslund A; Lubitz W; Siegbahn PEM; Högbom M. Direct Observation of Structurally Encoded Metal Discrimination and Ether Bond Formation in a Heterodinuclear Metalloprotein. Proc. Natl. Acad. Sci 2013, 110 (43), 17189–17194. 10.1073/pnas.1304368110. [PubMed: 24101498]

(18). Powell MM; Rao G; Britt RD; Rittle J. Enzymatic Hydroxylation of Aliphatic C–H Bonds by a Mn/Fe Cofactor. J. Am. Chem. Soc 2023, 145 (30), 16526–16537. 10.1021/jacs.3c03419. [PubMed: 37471626]

(19). Whittaker JW Non-Heme Manganese Catalase – The ‘Other’ Catalase. Arch. Biochem. Biophys 2012, 525 (2), 111–120. 10.1016/j.abb.2011.12.008. [PubMed: 22198285]

(20). Cotruvo JA; Stich TA; Britt RD; Stubbe J. Mechanism of Assembly of the Dimanganese-Tyrosyl Radical Cofactor of Class Ib Ribonucleotide Reductase: Enzymatic Generation of Superoxide Is Required for Tyrosine Oxidation via a Mn(III)Mn(IV) Intermediate. J. Am. Chem. Soc 2013, 135 (10), 4027–4039. 10.1021/ja312457t. [PubMed: 23402532]

(21). Rose HR; Ghosh MK; Maggiolo AO; Pollock CJ; Blaesi EJ; Hajj V; Wei Y; Rajakovich LJ; Chang W; Han Y; Hajj M; Krebs C; Silakov A; Pandelia M-E; Bollinger JM; Boal AK Structural Basis for Superoxide Activation of Flavobacterium Johnsoniae Class I Ribonucleotide Reductase and for Radical Initiation by Its Dimanganese Cofactor. Biochemistry 2018, 57 (18), 2679–2693. 10.1021/acs.biochem.8b00247. [PubMed: 29609464]

(22). Boal AK; Cotruvo JA; Stubbe J; Rosenzweig AC Structural Basis for Activation of Class Ib Ribonucleotide Reductase. Science (80-.). 2010, 329 (5998), 1526–1530. 10.1126/science.1190187.

(23). Coggins MK; Sun X; Kwak Y; Solomon EI; Rybak-Akimova E; Kovacs JA Characterization of Metastable Intermediates Formed in the Reaction between a Mn(II) Complex and Dioxygen, Including a Crystallographic Structure of a Binuclear Mn(III)–Peroxo Species. J. Am. Chem. Soc 2013, 135 (15), 5631–5640. 10.1021/ja311166u. [PubMed: 23470101]

(24). Lin YH; Kutin Y; Van Gastel M; Bill E; Schnegg A; Ye S; Lee WZ A Manganese(IV)-Hydroperoxo Intermediate Generated by Protonation of the Corresponding Manganese(III)-Superoxo Complex. J. Am. Chem. Soc 2020, 142 (23), 10255–10260. 10.1021/jacs.0c02756. [PubMed: 32412757]

(25). Shul’pin GB; Süss-Fink G; Shul’pina LS Oxidations by the System “Hydrogen Peroxide–Manganese(IV) Complex–Carboxylic Acid”: Part 3. Oxygenation of Ethane, Higher Alkanes,

Alcohols, Olefins and Sulfides. J. Mol. Catal. A Chem 2001, 170 (1), 17–34. https://doi.org/10.1016/S1381-1169(01)00052-8.

(26). Lane BS; Vogt M; DeRose VJ; Burgess K. Manganese-Catalyzed Epoxidations of Alkenes in Bicarbonate Solutions. J. Am. Chem. Soc 2002, 124 (40), 11946–11954. 10.1021/ja025956j. [PubMed: 12358539]

(27). Wang K; Mayer JM Oxidation of Hydrocarbons by [(Phen) 2 Mn(μ-O) 2 Mn(Phen) 2] 3+ via Hydrogen Atom Abstraction. J. Am. Chem. Soc 1997, 119 (6), 1470–1471. 10.1021/ja963180e.

(28). Liu C; Powell MM; Rao G; Britt RD; Rittle J. Bioinformatic Discovery of a Cambialistic Monooxygenase. J. Am. Chem. Soc 2024, 146 (3), 1783–1788. 10.1021/jacs.3c12131. [PubMed: 38198693]

(29). Kutin Y; Srinivas V; Fritz M; Kositzki R; Shafaat HS; Birrell J; Bill E; Haumann M; Lubitz W; Högbom M; Griese JJ; Cox N. Divergent Assembly Mechanisms of the Manganese/Iron Cofactors in R2lox and R2c Proteins. J. Inorg. Biochem 2016, 162, 164–177. 10.1016/j.jinorgbio.2016.04.019. [PubMed: 27138102]

(30). Zocher G; Winkler R; Hertweck C; Schulz GE Structure and Action of the N-Oxygenase AurF from Streptomyces Thioluteus. J. Mol. Biol 2007, 373 (1), 65–74. 10.1016/j.jmb.2007.06.014. [PubMed: 17765264]

(31). Choi YS; Zhang H; Brunzelle JS; Nair SK; Zhao H. In Vitro Reconstitution and Crystal Structure of P-Aminobenzoate N-Oxygenase (AurF) Involved in Aureothin Biosynthesis. Proc. Natl. Acad. Sci. U. S. A 2008, 105 (19), 6858–6863. 10.1073/pnas.0712073105. [PubMed: 18458342]

(32). Amyes TL; Richard JP Primary Deuterium Kinetic Isotope Effects From Product Yields: Rationale, Implementation, and Interpretation. In Methods in Enzymology; Elsevier Inc., 2017; Vol. 596, pp 163–177. 10.1016/bs.mie.2017.06.043. [PubMed: 28911770]

(33). Klinman JP; Offenbacher AR Understanding Biological Hydrogen Transfer Through the Lens of Temperature Dependent Kinetic Isotope Effects. Acc. Chem. Res 2018, 51 (9), 1966–1974. 10.1021/acs.accounts.8b00226. [PubMed: 30152685]

(34). Reed GH; Ray WJ Electron Paramagnetic Resonance Studies of Manganese(II) Coordination in the Phosphoglucomutase System. Biochemistry 1971, 10 (17), 3190–3197. 10.1021/bi00793a005. [PubMed: 4330325]

(35). Rusnak F; Yu L; Todorovic S; Mertz P. Interaction of Bacteriophage λ Protein Phosphatase with Mn(II): Evidence for the Formation of a [Mn(II)] 2 Cluster. Biochemistry 1999, 38 (21), 6943–6952. 10.1021/bi982606u. [PubMed: 10346916]

(36). Golombek AP; Hendrich MP Quantitative Analysis of Dinuclear Manganese(II) EPR Spectra. J. Magn. Reson 2003, 165 (1), 33–48. 10.1016/j.jmr.2003.07.001. [PubMed: 14568515]

(37). Cotruvo JA Jr.; Stubbe J. Metallation and Mismetallation of Iron and Manganese Proteins in Vitro and in Vivo: The Class I Ribonucleotide Reductases as a Case Study. Metallomics 2012, 4 (10), 1020–1036. 10.1039/c2mt20142a. [PubMed: 22991063]

(38). Teutloff C; Schäfer K-O; Sinnecker S; Barynin V; Bittl R; Wieghardt K; Lendzian F; Lubitz W. High-Field EPR Investigations of MnIIIMnIV and MnIIMnIII States of Dimanganese Catalase and Related Model Systems. Magn. Reson. Chem 2005, 43 (S1), S51–S64. 10.1002/mrc.1685. [PubMed: 16235205]

(39). Cox N; Ames W; Epel B; Kulik LV; Rapatskiy L; Neese F; Messinger J; Wieghardt K; Lubitz W. Electronic Structure of a Weakly Antiferromagnetically Coupled Mn II Mn III Model Relevant to Manganese Proteins: A Combined EPR, 55 Mn-ENDOR, and DFT Study. Inorg. Chem 2011, 50 (17), 8238–8251. 10.1021/ic200767e. [PubMed: 21834536]

(40). Haddy A; Waldo GS; Sands RH; Penner-Hahn JE Simulation of Multifrequency EPR Spectra from Mn(III)/Mn(IV) Catalase of Lactobacillus Plantarum Using a New Approach Based on Perturbation Theory. Inorg. Chem 1994, 33 (12), 2677–2682. 10.1021/ic00090a033.

(41). Ferroud C; Rool P; Santamaria J. Singlet Oxygen Mediated Alkaloid Tertiary Amines Oxidation by Single Electron Transfer. Tetrahedron Lett. 1998, 39 (51), 9423–9426. 10.1016/S0040-4039(98)02184-4.

(42). Adamenkov YA; Kalacheva AA; Shaidulina VA; Gorbunov MA Measurement of Singlet Oxygen Concentration in the Ambient Atmosphere. Russ. J. Rhys. Chem. A 2024, 98 (5), 953–956. 10.1134/S0036024424050029.

(43). Miyake N; Kim M; Kurata T. Formation Mechanism of Monodehydro-L-Ascorbic Acid and Superoxide Anion in the Autoxidation of L-Ascorbic Acid. Biosci. Biotechnol. Biochem 1997, 61 (10), 1693–1695. 10.1271/bbb.61.1693. [PubMed: 27393166]

(44). Scarpa M; Stevanato R; Viglino P; Rigo A. Superoxide Ion as Active Intermediate in the Autoxidation of Ascorbate by Molecular Oxygen. Effect of Superoxide Dismutase. J. Biol. Chem 1983, 258 (11), 6695–6697. 10.1016/S0021-9258(18)32271-3. [PubMed: 6304051]

(45). Hoang HM; Johnson HE; Heo J. Rac-Dependent Feedforward Autoactivation of NOX2 Leads to Oxidative Burst. J. Biol. Chem 2021, 297 (2), 100982. 10.1016/j.jbc.2021.100982. [PubMed: 34293347]

(46). Zou Y; Chen J; Liu X; Lu L; Davis RL; Jørgensen KA; Xiao W. Highly Efficient Aerobic Oxidative Hydroxylation of Arylboronic Acids: Photoredox Catalysis Using Visible Light. Angew. Chemie Int. Ed 2012, 51 (3), 784–788. 10.1002/anie.201107028.

(47). Whittaker MM; Barynin VV; Antonyuk SV; Whittaker JW The Oxidized (3,3) State of Manganese Catalase. Comparison of Enzymes from Thermus Thermophilus and Lactobacillus Plantarum. Biochemistry 1999, 38 (28), 9126–9136. 10.1021/bi990499d. [PubMed: 10413487]

(48). Barynin VV; Whittaker MM; Antonyuk SV; Lamzin VS; Harrison PM; Artymiuk PJ; Whittaker JW Crystal Structure of Manganese Catalase from Lactobacillus Plantarum. Structure 2001, 9 (8), 725–738. 10.1016/S0969-2126(01)00628-1. [PubMed: 11587647]

(49). Gama SR; Lo BSY; Séguin J; Pallitsch K; Hammerschmidt F; Zechel DL C–H Bond Cleavage Is Rate-Limiting for Oxidative C–P Bond Cleavage by the Mixed Valence Diiron-Dependent Oxygenase PhnZ. Biochemistry 2019, 58 (52), 5271–5280. 10.1021/acs.biochem.9b00145. [PubMed: 31046250]

(50). Wörsdörfer B; Lingaraju M; Yennawar NH; Boal AK; Krebs C; Bollinger JM; Pandelia M-E Organophosphonate-Degrading PhnZ Reveals an Emerging Family of HD Domain Mixed-Valent Diiron Oxygenases. Proc. Natl. Acad. Sci 2013, 110 (47), 18874–18879. 10.1073/pnas.1315927110. [PubMed: 24198335]

(51). Xing G; Diao Y; Hoffart LM; Barr EW; Prabhu KS; Arner RJ; Reddy CC; Krebs C; Bollinger JM Evidence for C–H Cleavage by an Iron–Superoxide Complex in the Glycol Cleavage Reaction Catalyzed by Myo -Inositol Oxygenase. Proc. Natl. Acad. Sci 2006, 103 (16), 6130–6135. 10.1073/pnas.0508473103. [PubMed: 16606846]

(52). Jodts RJ; Ho MB; Reyes RM; Park YJ; Doan PE; Rosenzweig AC; Hoffman BM Initial Steps in Methanobactin Biosynthesis: Substrate Binding by the Mixed-Valent Diiron Enzyme MbnBC. Biochemistry 2024, 63 (9), 1170–1177. 10.1021/acs.biochem.4c00011. [PubMed: 38587906]

(53). Sendra KM; Barwinska-Sendra A; Mackenzie ES; Baslé A; Kehl-Fie TE; Waldron KJ An Ancient Metalloenzyme Evolves through Metal Preference Modulation. Nat. Ecol. Evol 2023, 7 (5), 732–744. 10.1038/s41559-023-02012-0. [PubMed: 37037909]

(54). Barnese K; Gralla EB; Cabelli DE; Selverstone Valentine J. Manganous Phosphate Acts as a Superoxide Dismutase. J. Am. Chem. Soc 2008, 130 (14), 4604–4606. 10.1021/ja710162n. [PubMed: 18341341]

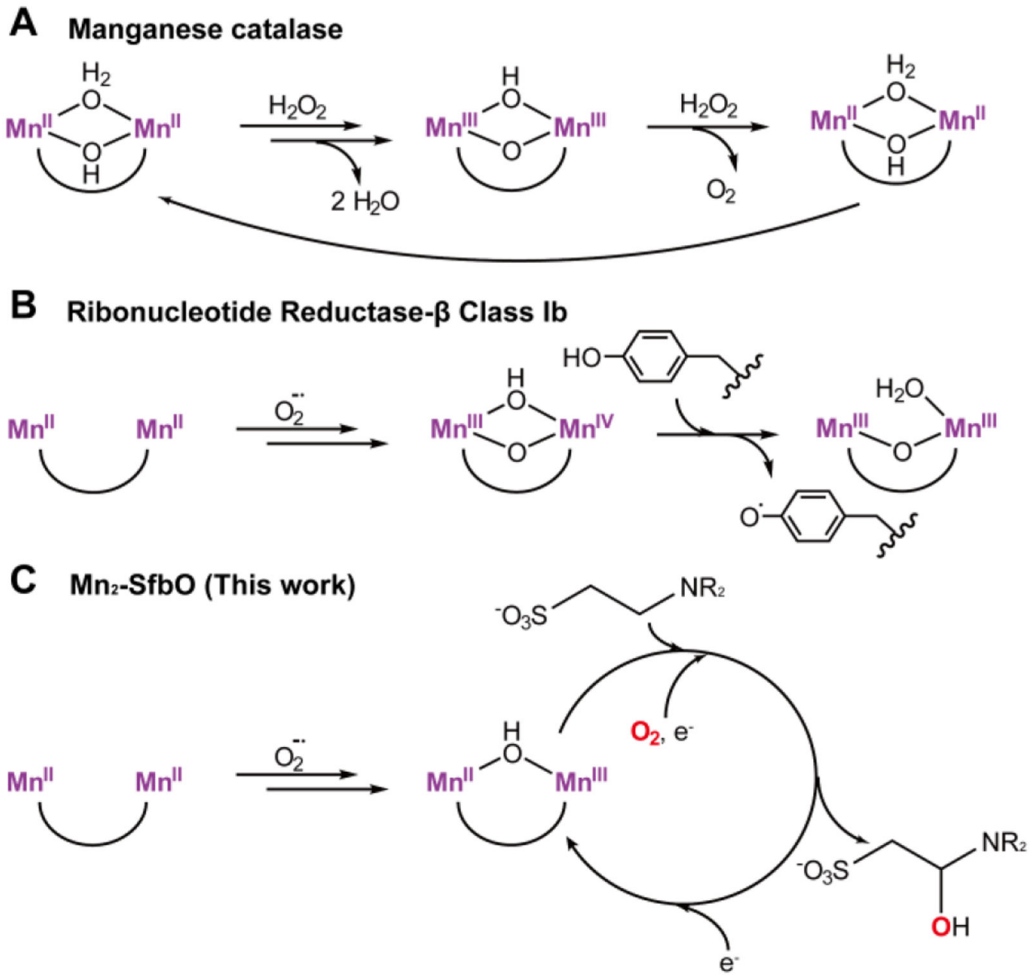

Figure 1.
Examples of redox-active dimanganese cofactors in biology.

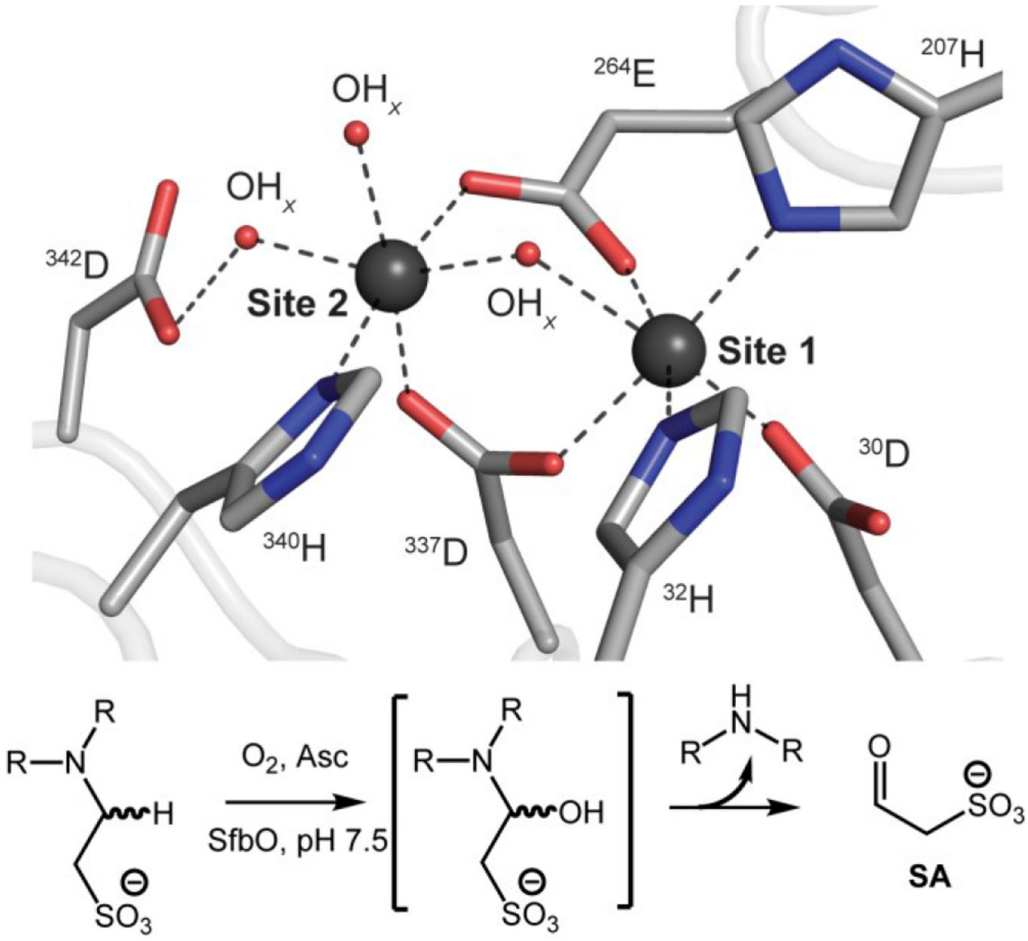

Figure 2.

(top) Cartoon representation of the dimetallic SfbO active site cofactor (PDB: 8SM6) and coordinating ligands, and (bottom) the proposed hydroxylation of β-aminoethyl-sulfonate-containing molecules by SfbO. OH_x represents a water derived ligand with unverified protonation state.

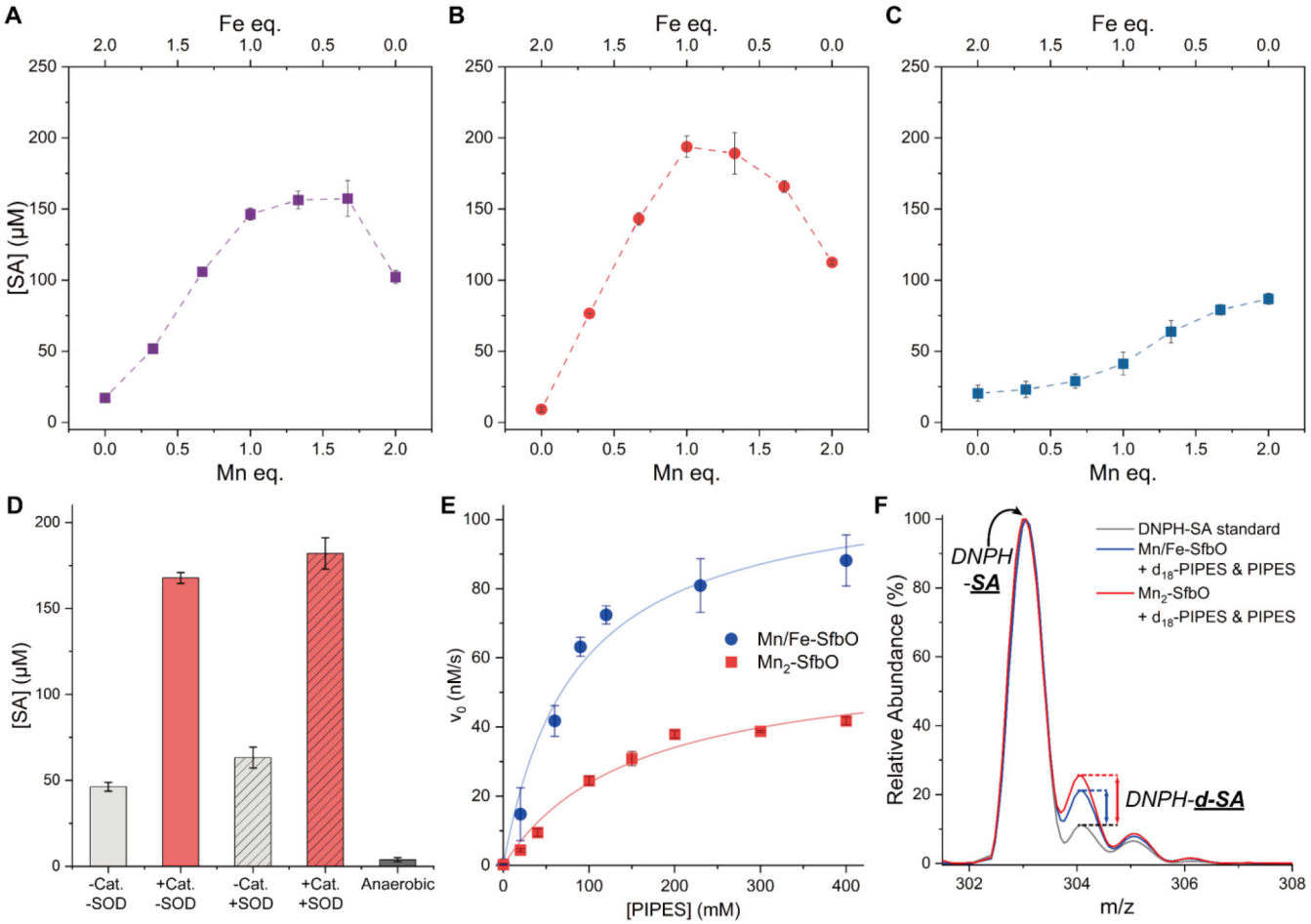

Figure 3.

Reactivity of SfbO metalated with 2 total equivalents of Mn^{II} and Fe^{II} per monomer, with (A) the Mn^{II} and Fe^{II} metal stock added simultaneously to the protein,[28] (B) Mn^{II} added prior to Fe^{II}, or (C) Fe^{II} added prior to Mn^{II}. (D) Comparative reactivity of Mn_2-SfbO in the presence of catalase or superoxide dismutase, or in the absence of oxygen. Standard reaction assay conditions (200 mM PIPES pH 7.25, 2 mM sodium ascorbate, 0.5 μM Mn_2-SfbO, supplemented with 0.05 mg/ml catalase or 0.1 mg/ml SOD if included) were used. The reactivity was evaluated by the concentration of SA product generated. The assays were performed in triplicate and the error bar represents the standard deviation. (E) Michaelis–Menten plot of the Mn_2-SfbO reaction with PIPES (K_M = 153 mM and k_{cat} = 0.06 s^{-1}), compared to Mn/Fe-SfbO.[28] (F) LCMS analysis of Mn_2- and Mn/Fe-SfbO reaction with 150 mM PIPES and d_{18}-PIPES for KIE calculations as described in Figures S2-3. The SA product was derivatized with DNPH to form DNPH-SA for quantification, as described in the methods section (Figure S2).

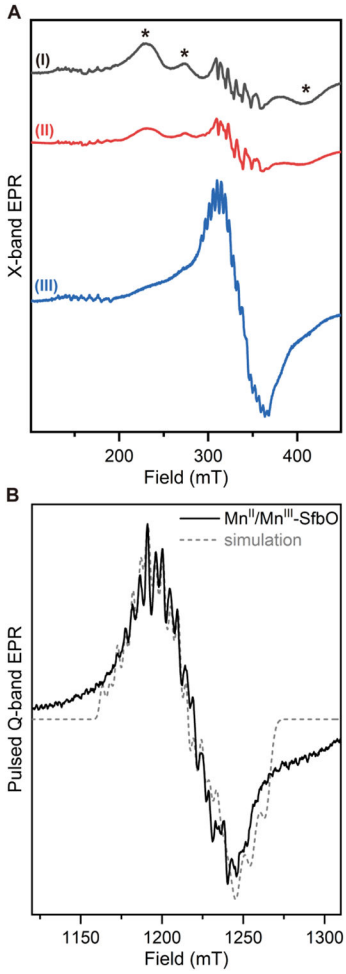

Figure 4.

(A) Continuous-wave X-band EPR spectra of (I) Mn_2^{II}-SfbO, (II) Mn_2^{II}-SfbO exposed to air overnight, (III) air-oxidized Mn_2-SfbO with 20 mM sodium dithionite added anaerobically. The features annotated with asterisks are attributed to excited state transitions of weakly antiferromagnetically coupled Mn_2^{II} species. (B) Pulsed Q-band EPR spectrum of $Mn^{II}Mn^{III}$-SfbO (Q-band pseudo-modulated electron spin-echo detected EPR, Figure S6).

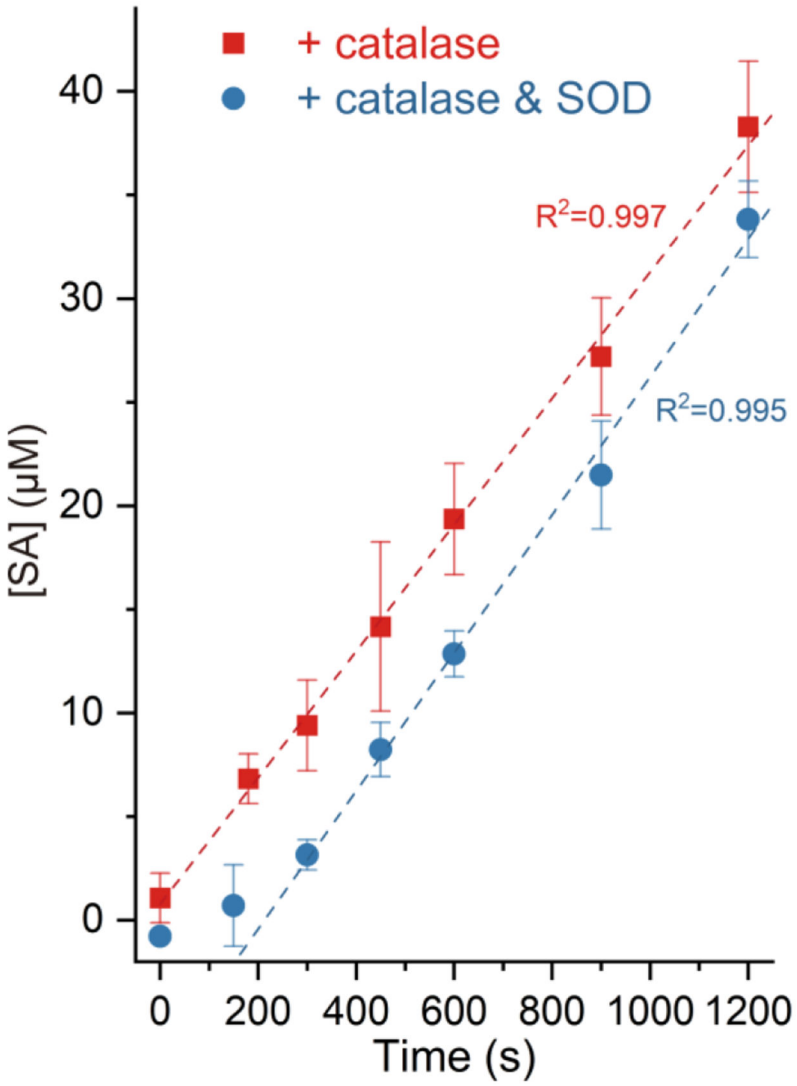

Figure 5.

Initial reaction profiles of Mn_2^{II}-SfbO performed in the presence of SOD and/or catalase. The assay components except SfbO (200 mM PIPES, 2 mM sodium ascorbate, 0.05 mg/ml catalase, and 0.1 mg/ml SOD if included) were mixed aerobically and incubated for 10 min before addition of the anaerobically prepared Mn_2^{II}-SfbO.

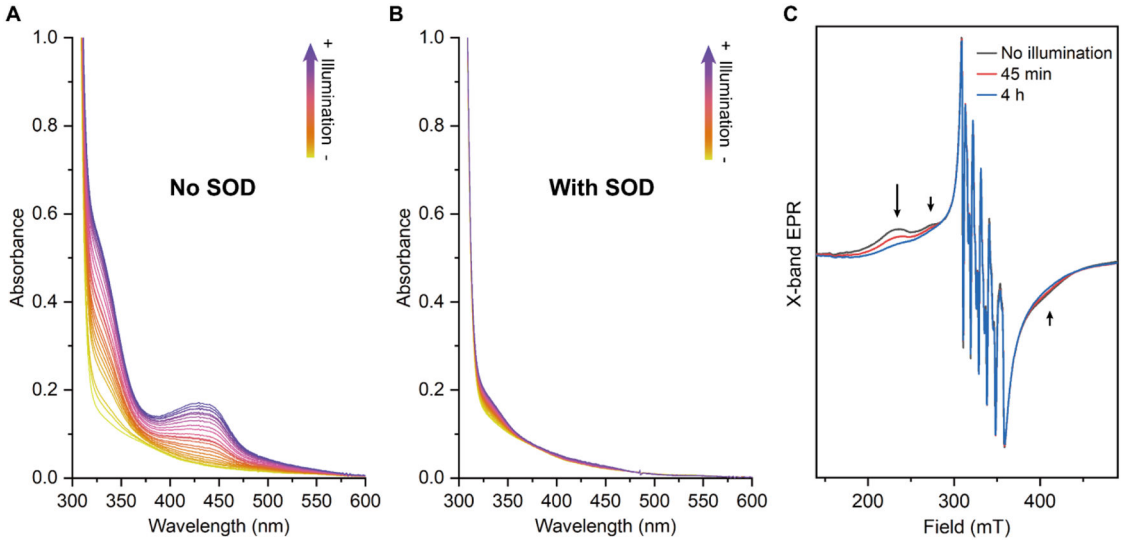

Figure 6.

Spectral changes following superoxide maturation of Mn_2^{II}-SfbO. (A) UV/visible spectra of 430 μM Mn_2^{II}-SfbO and 2 equivalents of supplemental Mn^{2+} aerated for 10 min before 5 mM iPr_2NEt and 5 μM $Ru(bpy)_3^{2+}$ was added. The UV/visible spectrum of the mixture was monitored over the course of illumination. (B) Duplication of the experiment shown in (A) in the presence of additional 2500 units/ml SOD. The absorbance of $Ru(bpy)_3^{2+}$ was subtracted in panels (A) and (B). (C) Light-dependent reaction of Mn_2^{II}-SfbO catalyzed by $Ru(bpy)_3^{2+}$ monitored by EPR. Each sample was taken from the same mixture solution containing 342 μM Mn_2^{II}-SfbO aerated for 10 min, supplemental Mn^{2+}, 10 μM $Ru(bpy)_3^{2+}$ and 10 mM iPr_2NEt, and was illuminated for the specified time.

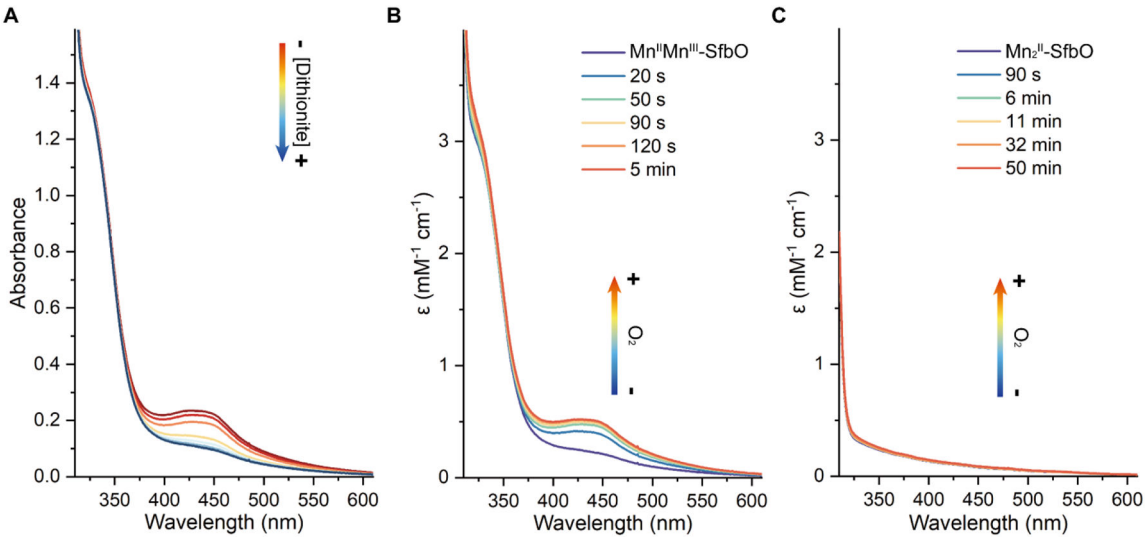

Figure 7.

UV/visible spectra of (A) Mn_2^{III}-SfbO titrated with DT and exposure of $Mn^{II}Mn^{III}$-SfbO to air (B). (C) Air exposure of Mn_2^{II}-SfbO monitored for 50 minutes.

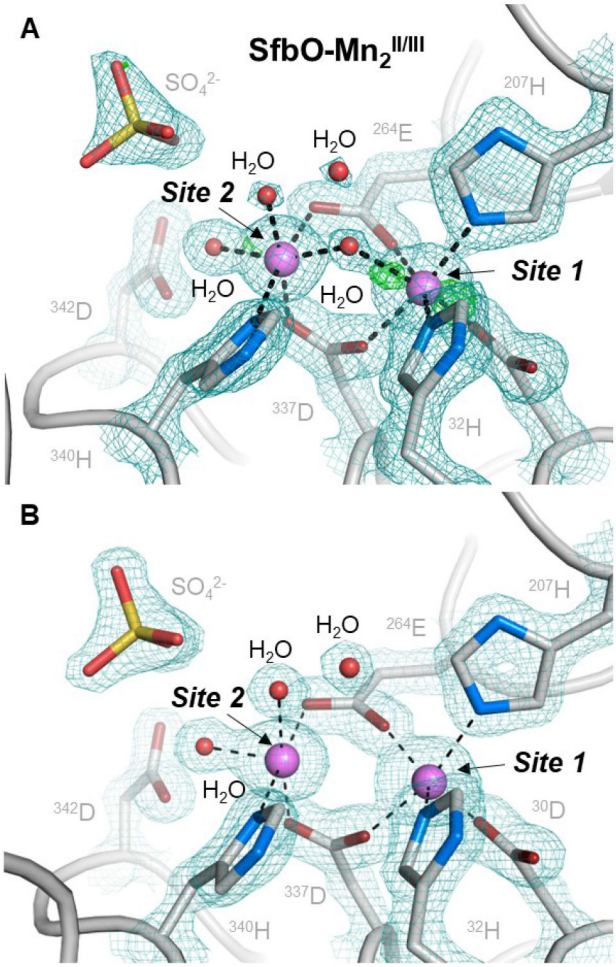

Figure 8.

Close-up views of the Mn_2 cofactors in $Mn^{II}Mn^{III}$-SfbO (**A**) and Mn_2^{II}-SfbO (**B**). The $2F_o–F_c$ maps are shown in teal (2.0σ) and the $F_o–F_c$ map in green/red (+/−4.0σ).

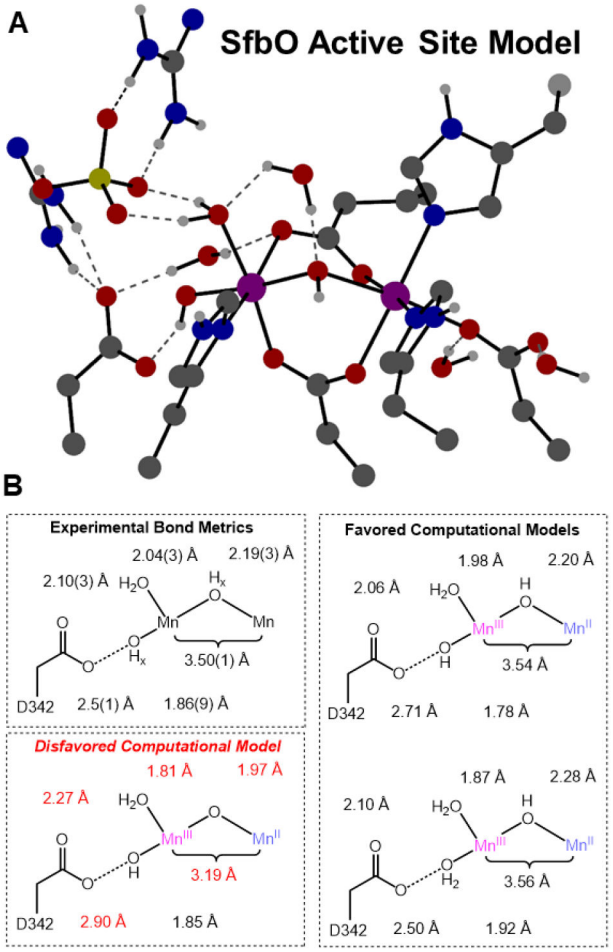

Figure 9.

(A) DFT-optimized geometry of the Broken Symmetry S_{TOT} = ½ $Mn^{II}Mn^{III}$ cofactor harboring a bridging hydroxide ligand and a terminal hydroxide bound to the Site 2 Mn^{III} ion. (B) Comparison of salient bond distances of the $Mn^{II}Mn^{III}$ cofactor obtained via XRD and three DFT models. Numbers in parentheses reflect the standard deviation obtained by comparing the 4 crystallographically-independent active sites.